Modeling of Neonatal Skull Development Using Computed Tomography Images

M. Mohtasebi, M. Bayat, S. Ghadimi, H. Abrishami Moghaddam, Fabrice Wallois

Modeling of Neonatal Skull Development Using Computed Tomography Images

Mehrana Mohtasebi[1], Mohammadreza Bayat[1], Sona Ghadimi[1,2], Hamid Abrishami Moghaddam[1,2], Fabrice Wallois[2,3]

[1] Faculty of Electrical Engineering, K.N. Toosi University of Technology, Tehran, Iran
[2] Inserm UMR 1105, Faculté de Médecine, Université de Picardie Jules Verne, Amiens, France
[3] Inserm UMR 1105, Centre Hospitalier Universitaire d'Amiens, Amiens, France

*** Correspondence:**

Hamid Abrishami Moghaddam

C.U.R.S. (Centre Universitaire de Recherche en Santé)
Université de Picardie Jules Verne
Pôle E (INSERM U1105-GRAMFC)
CHU Sud (Centre Hospitalo-Universitaire)
Avenue Laënnec
80054 Amiens, France

Email: hamid.abrishami@u-picardie.fr
Tel : +33 322 825382
Fax : +33 322 825381

1 Introduction

The ability to determine the normal progress of skull morphological development in neonates is clinically important to monitoring prenatal and postnatal brain growth because abnormalities in brain growth may cause neurological disorders in neonates. Moreover, the effects of uncertainty in head tissue conductivity and complexity on EEG and MEG forward modeling in neonates have been previously demonstrated by a number of studies [1, 2]. The neonatal skull has many characteristic features compared to an adult skull. In neonate, the bony plates of the skull connect to each other via fontanels and sutures to compose the skull. Fontanels are the fibrous, membrane-filled gaps appearing where more than two cranial bones are juxtaposed, as opposed to sutures, which are narrow seams of fibrous connective tissue that separate the flat bones of the skull [3]. The fontanels and sutures permit bones moving as the infant passes through the birth canal. Normally, the growth of the brain and skull (including normal closure of fontanels and sutures) are tightly linked and regulated, but there are conditions in which this balance is not maintained. Premature ossification or delay in the closure of the fontanels and sutures can cause abnormalities in the brain [4]. Palpation of neonate's fontanel by the pediatrician for examining newborn healthiness is a subjective task depending on pediatrician's skill and experience. Nevertheless, a subtle quantitative and qualitative assessment of neonate's skull shape and size during early infancy has a crucial role in identifying an underlying brain malformation and skull deformation.

Magnetic resonance imaging (MRI) and computed tomography (CT) are two predominant modalities used in the head clinical examinations. MRI has the advantage of being nonionizing due to using a magnetic field and radio waves for imaging. While this modality demonstrates superior soft tissue contrast with high precision, it is not suitable for accurate skull detection, especially in newborns who have a very thin skull. In contrast, CT is optimally employed for imaging hard tissues and therefore contributes to evaluating skull structures. Accordingly, CT scans are employed as the imaging modality of choice for skull study in this paper. CT scans in this research were acquired from neonates that had been already prescribed for routine diagnostic purposes whereas later examinations affirmed their healthiness. Fontanels and sutures in CT images are barely seen as a tissue with an identifiable gray level. They are simply distinguished from other tissues as gaps between cranial bones. Ghadimi et al. [5] proposed a method based on the variational coupled level sets to segment and reconstruct cranial bones, fontanels and sutures from neonatal CT images. Using their method, the fontanels and sutures' size and area can be determined based on real head model. There is a relative paucity of literature focusing on the neonatal skull development by using real head model. Some published articles elucidate the anatomical development of skull structure by reviewing some CT examinations [6] or by using a limited number of cranial landmarks [7, 8].

Techniques for understanding and monitoring the process of skull development across populations of neonates mostly require age-appropriate neonatal average models or atlases as reference to spatially normalize data to a stereotactic space. Atlases depict general anatomical features of the under-study population and can be built and utilized as a priori knowledge to perform morphological development analysis of neonates within a particular age interval. Specifically, neonatal head atlases are utilized as important tools in studying global and regional growth of brain

structure and function, detecting specific disease or atrophy in structures and applying model-based segmentation [9-11]. An important additional advantage of templates is employing them to detect and quantify local abnormalities by measuring the variations in anatomy between a template and individual subjects.

A number of approaches have been presented for construction of neonatal CT template in full alignment with neonatal MR template [12, 13]. Ghadimi et al. [13] provide a CT template with high spatial resolution that is appropriate for dense characterization of skull development in neonates. The constructed CT template is in a standard stereotaxic space similar to MNI which could be used for spatial normalization in CT modality.

Due to the rapid changes and marked heterogeneity inherent to the developing brain [9], it is critical to consider a reasonably limited age range of neonates under-study to analyze local anatomical features [14]. Momeni et al. [15] construct two templates for the gestational age (GA) ranges of 39 to 40 and 41 to 42 weeks using T1-weighted MR images. They estimate the temporal resolvability of macroscopic anatomical changes due to the brain development in neonates. Then, they compare the spatial variation of anatomical landmarks, the average and the maximal length of spatial deformation in 30 subjects that were normalized to the two templates. The results strengthened the hypothesis that two-week is the temporal resolvability of age-related templates for macroscopic morphological studies of the developing brain and revealed significant differences between spatial variations of the above macroscopic features in the two mentioned age ranges.

In the current study, two neonatal head CT templates in narrower age ranges are created. Two-week temporal resolvability in the ranges of 39 to 40 and 41 to 42 weeks GA is considered for developing age related CT templates based on the study by Momeni et al. [15]. These templates can indicate anatomy, structures characteristic or regional growth for the population. Moreover,

these templates are created for the first time in a standard anatomical coordinate system using a relatively large population of subjects in each age range. They provide higher spatial and temporal resolution required for dense characterization of skull development in neonates. For qualitative evaluation of skull growth, the deformation field derived from alignments between templates at different time intervals and from intra-subject registrations to a common space are utilized to calculate Jacobian determinant matrix. Jacobian determinants indicate the skull developmental changes between two age ranges under-study. Afterwards, we present quantitative assessments of skull growth including determination of head circumference, size of anterior and posterior fontanels, cranial bones, fontanels and sutures surface area.

2 Materials and Methods

The proposed methodology includes 5 stages: I) data pre-processing; II) intensity transform; III) mapping images to neonatal MR template; IV) creating age specific neonatal templates; and V) skull development analysis.

After data preprocessing and intensity transformation stages, the CT images were mapped to an available MR template. The MR template represents the standard coordinate system within which the CT templates are constructed. Therefore, the full alignment of CT images with the MR template is essential. Then, two age related CT templates (in the age ranges of 39-40 and 41-42 weeks GA) were built. Constructing age-specific CT templates are required since the scans must be mapped to a common space in order to be anatomically comparable. Moreover, the neonatal CT head templates consider the effects of variability in neonates' head geometry in the cohort at each time-interval. They are useful to estimate population or region-specific growth patterns and to visualize neonatal skull anatomy.

2.1 Subject and data acquisition

The newborn CT images were selected from a database acquired during recent years at Amiens University Hospital, France, which is a regional referral, subspecialty care center. CT images were reviewed by a pediatric neuroradiologist and 19 subjects between 39 and 42 weeks GA with neither anatomical abnormalities nor mismatch between their chronological age and developmental progress were selected. The images in DICOM format were acquired using a LightSpeed 16, GE Medical Systems, with a matrix size of 512×512 pixels and converted to analyze format. Table 1 shows the detailed information including sex, GA (at the date of exam and at the date of birth) and CT image resolution for each subject.

Table 1. Describing the subjects by their sex, ages at the date of birth and exam and their CT image voxel size.

Subjects	Gender	GA at date of exam (w)	GA at date of birth(w)	Voxel size (mm^3)	Subjects	Gender	GA at date of exam (w)	GA at date of birth (w)	Voxel size (mm^3)
S1	F	39w	36w	0.33×0.33×0.63	S11	F	41w5d	41w	0.35×0.35×0.63
S2	F	39w	37w	0.31×0.31×0.63	S12	M	41w6d	41w	0.49×0.49×0.63
S3	F	39w1d	39w	0.26×0.26×0.6	S13	M	42w	29w	0.35×0.35×1.25
S4	M	39w3d	39w	0.27×0.27×0.63	S14	M	42w	34w	0.31×0.31×0.6
S5	M	40w	32w	0.37×0.37×0.63	S15	M	42w	34w	0.35×0.35×0.63
S6	M	40w	39w2d	0.29×0.29×0.63	S16	F	42w	38w	0.29×0.29×0.63
S7	M	40w2d	28w2d	0.31×0.31×0.63	S17	M	42w	38w	0.36×0.36×0.6
S8	F	40w6d	40w	0.35×0.35×0.63	S18	M	42w1d	40w	0.33×0.33×0.63
S9	M	41w	34w	0.36×0.36×1.25	S19	M	42w4d	37w4d	0.27×0.27×0.63
S10	M	41w2d	41w	0.29×0.29×0.6					

GA: gestational age, w: weeks, d: day(s), F: Female, M: Male

2.2 Data preprocessing

An important preprocessing step for reducing the intra-subject anatomical variability is spatial normalization mapping to a reference frame. One of the bases for a coordinate system could be Reid's base line (RBL) or the so-called Frankfurt plane, which was established in 1884 as the

anatomic position of the human skull. RBL is passing through the lowest border of the orbit and the upper border of the external acoustic meatus whose normal lies on the mid-sagittal plane [16, 17]. Radiologists also defined canthomeatal line (CML) which is passing through the two lateral angles of the eyes and the center of the external acoustic meatus; this plane lies approximately 10 degree nose up to the Frankfort plane. However, it is not possible to draw RBL and CML on the brain. Moreover, the use of these planes presumes strict symmetry of the skull which can be seen in only 10% of the cases [17]. In the majority of cases, the internal auditory meatuses are located in different planes, and the interaural line (the straight line between the points of earbars in the external auditory meatus of each ear) and midplanes, as well as Reid's plane, are not rigorously perpendicular to each other. This nullifies the localizing value of these planes [17]. However, the Talairach space, a standard 3-dimensional coordinate system of the brain is commonly used as a target space for normalization mapping. Generally, spatial normalization to Talairach space is performed by specifying landmarks like anterior commissure (AC) and posterior commissure (PC) in the image and then applying Talairach transformation to adjust position, orientation and size of an individual brain [18]. The AC-PC line is almost parallel to the CML and shows approximately 15 degrees difference from the RBL [16]. An alternative approach is normalizing the image to a template that has been previously constructed in Talairach space. Although a CT scan provides the best contrast for cranial bones, its low contrast for soft tissue makes detecting AC and PC landmarks practically impossible. Consequently, in order to build age-specific neonatal CT templates in Talairach space, we chose to use the latest approach and align our CT images with a neonatal MR template that was previously constructed in the age ranges under-study, and also built upon the Talairach coordinate system. So all the 19 CT images in the dataset were mapped to the neonatal MR brain template known as 'GRAMFC_$T_{39\text{-}42}$' [19] with GA between 39-42 weeks by

applying a hybrid method which uses both intensity and feature information for intra-subject intra-modality registration similar to the method proposed by Ghadimi et al. [13]. This template was built in a way that AC is placed at the origin and the AC-PC line is in the horizontal plane so its origin and axes are based on Talairach coordinates. GRAMFC_$T_{39\text{-}42}$ also concerns the whole head and contains the skull layer, which is the feature of special interest for normalizing our whole head CT images to its space.

For CT to MR alignment, the manual linear normalization was performed first via the "Transformation" module in 3D Slicer software [20]. This module provides the ability to translate and rotate images to roughly align them with the reference space. Subsequently, by using "CropVolume" module in this software, any excess signals from neck and sides of the head are omitted and the clean head image is obtained. Applying rigid transformations by 3D Slicer on CT images cause some of the background voxels to be set to zero intensity. As typical CT scans were calibrated using Hounsfield units (HU), these voxels in the background are misinterpreted as water (CSF) due to their zero intensity. In addition to these disruptive signals, there exist other factors that produce excess signal in CT images. One of them is an artificial rim with the intensity of -3000 around air produced by some GE scanners, while any voxel outside the head in the background gets air intensity (-1000 HU). Other types of disruptive signals in CT images are produced by the patient's accessory during scanning such as anesthesia mask, vacuum pillow (for fixing their head and eliminating motion artifacts), or in some cases, nasogastric or orogastric feeding tube. Using a CT head mask is helpful to get rid of these undesirable signals. CT head mask was extracted by applying Otsu's thresholding method [21] on a CT image histogram and then excess signals on CT head mask were eliminated using morphological operators. It is noteworthy that the rigid transformation provided by manual alignment in 3D Slicer for each CT

image was applied to its corresponding head mask. All the voxels outside the head were considered as air with the intensity value of -1000 by using the head mask.

2.3 Intensity transform

Precise registration methods are required to create a CT template in the stereotaxic space defined by GRAMFC_T_{39-42}. Since CT scans must be co-registered to a template in MR modality, the intensities of CT scans were modified using the method proposed by Rorden et al. [22] to widen soft tissue dynamic range and ameliorate its contrast to improve co-registration result. Normalizing CT scans by using intensity-based registration (as in this study), would be primarily triggered by the contrast of air (~-1000 HU) and bone (~1000 HU) and therefore soft tissues like brain structures would not be aligned effectively with each other. For this purpose, the intensity values from -1000 to -100 were transformed to 0-900 by adding +1000, values from -99 to 100 were linearly scaled to the range of 911 to 3100 and the intensities higher than 100 ($I > 100$) were converted to $I + 3000$.

2.4 Mapping images to neonatal MR template

The procedure used here for the construction of the neonatal CT template is similar to the approach proposed in our recent work [13] for the creation of neonatal bimodal MR-CT template. The intensity transformed CT scans were registered to MR template in two steps: 1) The intracranial parts of CT image were registered nonlinearly to MR intracranial template and the resultant deformation field was applied to the whole CT image, 2) The whole registered CT image derived from the first step was registered linearly to the MR template.

First the intracranial parts of CT images including brain, CSF and dura matter (Figure 1A) were extracted to be aligned with MR intracranial template (Figure 1B) created by Ghadimi et al. [13]. The CT intracranial was extracted using the coupled level sets algorithm for skull segmentation

and fontanels reconstruction [5] applied to the intensity transformed CT scans. The algorithm is based on the variational coupled level set and has been developed for the extraction of new born skull including fontanels and sutures from CT images. Beside segmentation, the method is designed to have surface reconstruction properties. This approach applies a pair of interior/exterior surfaces as geodesic active regions propagating towards and interacting with each other. The moving surfaces are forced to stop alongside of the outer (convex) and inner (concave) surface of cranial bones using edge information. By considering the corresponding mask of the resulted interior contour, the CT intracranial was extracted.

Advanced Normalization Tools software (ANTs) [23] was utilized for automatic normalization between intracranials. ANTs is an open source toolkit software implemented based on Insight ToolKit (ITK) framework [24]. The automatic normalization procedure included a 12-parameter affine transformation (rotations, translations, zooms and shears, each in 3 dimensions), followed by a nonlinear deformation. The affine transformation determines the optimal compression/expansion for fitting overall shape and size, and the nonlinear deformation accounts for smaller scale anatomical differences. Nonlinear deformation was applied by using symmetric normalization transformation (SyN) [25] algorithm implemented in ANTs by running *antsRegistration* script and defining mutual information (MI) as its cost function.

After co-registering MR and CT intracranials (Figure 1C), the affine matrix which resulted from linear registration and the warping field which resulted from nonlinear registration using SyN were applied to the whole intensity transformed CT image. Hereafter, the notation CT' refers to CT image resultant from the previous step (Figure 1D). In the second step, in order to take advantages of extracranial part of the head, an affine registration was carried out between MR template (Figure

1E) and the CT' image. The resulted registered CT scans (Figure 1F) matched quite well to the GRAMFC_$T_{39\text{-}42}$ template and they were utilized as input for template building.

2.5 Age related neonatal template construction

ANTs provides a template construction function by using optimal groupwise registration that derives an optimal unbiased template with respect to both shape and appearance according to the input images [26]. In this method, the optimal groupwise registration is executed by iteratively constructing the initial template and estimating the transformation fields of all subjects towards the estimated initial template without any bias effect of the individual subject as reference. This symmetric groupwise normalization (SyGN) method is available in ANTs software via the script *antsMultivariateTemplateConstruction.sh* [25, 27]. It was run for two iterations using its default similarity measure and SyN energy term to construct age related CT templates.

By constructing age related templates for neonates, we are also able to create cranial bone probability map. At first, cranial bones were segmented by automatic thresholding using Otsu's method [21] on CT images. Then, extracted cranial bones for each individual were transformed into the age-related template's space by applying the transformation parameters obtained during template creation. Finally, the normalized cranial bones were averaged and smoothed with a Gaussian filter.

2.6 Skull development analysis

In order to assess the skull growth in neonates in the age ranges of 39 to 40 and 41 to 42 weeks GA, three different scenarios were considered. In the first scenario, two unbiased CT templates were constructed using the proposed algorithm in the previous sections. They represent the common anatomy and anatomical variations within the groups in the age ranges of 39-40 ($CT_{39\text{-}40}$) and 41-42 ($CT_{41\text{-}42}$) weeks GA. Then the template at the age ranges of 39-40 was registered to

the template at the age range of 41-42 using nonlinear SyN transformation. Deformation-based morphometry (DBM) [28] was applied to calculate anatomical differences between groups in time and space. Deformation field was calculated from the gradients of 3D non-linear volumetric warping. After applying nonlinear SyN transformation to normalize $CT_{39\text{-}40}$ to $CT_{41\text{-}42}$, the ANTs' script *ComposeMultiTransform.sh* was used for combining the affine and warp deformation matrices estimated from non-linear registration into one deformation field matrix. Then, the Jacobian matrix in each 3D point was computed using this deformation field. The Jacobian determinants were interpreted as local contraction ($|J| < 1$), local expansion ($|J| > 1$) and no volume changes ($|J| = 1$) [10].

In the second scenario, a global average CT template was built for the neonates at the age ranges of 39-42 weeks GA ($CT_{39\text{-}42}$). For this purpose, the CT template creation algorithm presented in the previous section was applied to the pool of all subjects. Then each individual was non-linearly normalized to $CT_{39\text{-}42}$ and the resulted deformation field was used for determining local differences between each individual and the global average CT template. In a similar way as in the first scenario, Jacobian determinants were calculated using the deformation field matrix of each subject. Finally, the average of Jacobian determinants corresponding to subjects in each group (39-40 and 41-42 weeks GA) was calculated. The resulted 3D matrices represent growth-related local changes in size or shape of neonates' skull. They were overlaid onto global average CT template for a qualitative assessment of normal neonatal skull growth.

In the third scenario, the normal neonatal skull growth patterns were evaluated quantitatively. For this purpose, the coupled level set approach for skull segmentation and fontanel reconstruction [5], was applied to the CT images derived from data preprocessing step (Section 2.2). This approach applies a pair of interior/exterior surfaces as geodesic active regions propagating towards and

interacting with each other. Level set evolution is stopped when they touch each other or encounter the outer (convex) and inner (concave) surfaces of cranial bones. In locations corresponding to fontanels and sutures, these moving surfaces touch each other without crossing over (Figure 2B). A mask of the inner surface was created by the filling operator (Figure 2C), and its volume was considered as intracranial volume. The area of resulting outer surface of cranial bones, fontanels and sutures was considered as the skull's surface area. The maximum length of outer contour in axial view was measured and considered as a scalp eliminated head circumference. After expert revision of the reconstructed fontanels and sutures, the anterior fontanel was segmented manually for each subject. The diamond-shaped anterior fontanel was found at the junction of the coronal, metopic, and sagittal sutures. The largest fontanels and sutures between cranial bones in coronal and sagittal view were assumed to be anteroposterior and transverse diameter respectively. The anterior fontanel size was derived (according to Popich and Smith's definition [29]) by averaging the length (anteroposterior dimension) and the width (transverse dimension) as presented in Figure 3. The knowledge of the size of anterior fontanel as the largest fontanel is useful for clinical examination and diagnosis of the abnormalities in intracranial and brain growth. The size and surface area of anterior fontanel and closure of the anterior fontanel in different age periods were determined by considering term and preterm infants, sex, growth parameters, gestational age and race [30, 31]. The ratio of the fontanels and sutures area to skull surface area (including bones and cartilage) can be used to determine the degree of ossification. Its value for an embryo without any ossified bones is equal to 1 and decreases to 0 at an age of about 2 years old when bone ossification is completed, and the majority of sutures are fused. In clinical assessment, the head circumference or occipital frontal circumference (OFC) is determined with a flexible calibrated non-stretchable plastic tape around the infant's head, specifically the most prominent part on the back of the head

(occiput) to just above the eyebrows (supraorbital ridges). In this study, the head circumference was measured by considering the largest circumference in axial plane.

3 Results

Figure 4 shows 3D surface visualization of the cranial bone probability map and reconstructed fontanels and sutures of the age-related CT templates. As shown in Figure 4, most sutures are being fused slightly after 2 weeks GA during fetal and postnatal life . The anterior fontanel size is larger in $CT_{41\text{-}42}$ with respect to $CT_{39\text{-}40}$. This finding appears to be clinically plausible; since in that region, the frontal white matter exhibits rapid expansion [9] which causes expansion in the anterior fontanel as well. The growth maps calculated by the first and second scenario are shown in Figures 5 and 6, respectively. The determinant of Jacobian matrices derived from deformation field of normalizing $CT_{39\text{-}40}$ template to $CT_{41\text{-}42}$ is overlaid on the three dimensional space of $CT_{41\text{-}42}$ in Figure 5. Jacobian determinant values less than one indicate the areas like occipital bone and lambdoid sutures which have contraction volume with respect to $CT_{41\text{-}42}$. The volume expansion of metopic sutures and majority of fontanels, especially anterior fontanel, demonstrates an increase in the size of fontanels in $CT_{41\text{-}42}$ with respect to $CT_{39\text{-}40}$ due to the expansion of white matter in the anterior areas in front of the ventricles. The first and second row in Figure 6 show the three dimensional overlay of the average Jacobian matrix determinants corresponding to 39-40 and 41-42 weeks GA subjects normalized to $CT_{39\text{-}42}$ template, respectively. The first row in Figure 6 shows no volume contraction around specific fontanels or sutures. In contrast, it shows volume expansion around sagittal sutures and all six fontanel spots including anterior, posterior, sphenoid and mastoid fontanels. The second row in Figure 6 shows volume contraction around most of the sutures except the sagittal one. There is volume expansion around posterior fontanel and sagittal sutures, but its value is not as large as for subjects at 39-40 weeks GA.

The anteroposterior and transverse skull diameters for each CT image, anterior fontanel size and anterior fontanel area are indicated in Table 2. The surface area of total fontanels and sutures tissue was measured and the ratio of anterior fontanel area to the total fontanels and sutures area is also reported in Table 2.

Table 2. Means ± Standard deviations of anterior fontanel size, scalp eliminated head circumference, area corresponding to fontanels and sutures, the ratio of fontanels area to outer surface of the skull and intracranial volume for the neonates in the age ranges of 39-40 and 41-42 weeks GA.

	39-40 weeks GA	41-42 weeks GA
Anteroposterior diameter of anterior fontanel (cm)	2.61±0.44	3.45±0.93
Transversal diameter of anterior fontanel (cm)	2.88±0.57	3.45±0.49
Anterior fontanel size (cm)	2.74±0.45	3.45±0.57
Anterior fontanel area (cm^2)	9.02±2.85	14.1±4.28
Total fontanels and sutures area (cm^2)	52.62±28.83	60±19.29
Anterior fontanel area / Total fontanels and sutures area	0.19±0.07	0.25±0.09
Skull surface area (cm^2)	618.3±53.32	692.71±46.89
Intracranial volume (ml)	441.68±71.58	512.09±50.38
Total fontanels and sutures area / Skull surface area	0.083±3.87	0.087±3.19
Scalp eliminated head circumference (cm)	30.2±1.63	31.09±2.34

Figure 7 shows anterior fontanel area in pink and total fontanel and sutures except anterior fontanel in blue. The individual anteroposterior and transversal diameter of anterior fontanel and their average (anterior fontanel size) are given in Figure 8. The scatter plot of individual intracranial volume is shown in Figure 9.

4 Discussion

We investigated patterns of skull maturation from a cohort of 19 infants. Our data set was composed of 8 and 11 CT images of newborns at the age ranges of 39 to 40 and 41 to 42 weeks GA, respectively (Table 1). In this paper, for the first time, we presented unbiased age-related CT head templates for healthy neonates with a gestational age of 39 to 40 and 41 to 42 weeks GA. The templates have various applications such as providing the reference spaces required for the studies on brain and skull or being used in pathological examinations which require precise geometry of the head including cranial bones, fontanels and sutures. The deformation based morphometry method was applied to analyze volumetric changes of skull structures by warping each subject to a common coordinate system represented by the templates. The normal limits of skull variation for the neonates at the given age ranges were shown qualitatively in Figure 5 and 6 and quantitatively in Table 2. The first row of Figure 6 shows the volume expansion around sagittal sutures and all six fontanel spots including anterior, posterior, sphenoid and mastoid fontanels. The anterior fontanel expanded due to the maturation of white matter and gray matter in the anterior areas in front of the ventricles. This volume expansion is indicative of an overall regional growth that was faster than the fontanel closure at the metopic and coronal sutures [7]. Findings from the current study shed light on skull development simultaneously with brain maturation. These results complement previous early postnatal period studies of infant brain or skull development [6, 7, 10, 31]. Mercan et al. [7] modeled the post-natal (0–6 months old) growth patterns of the skull in both normative and sagittal craniosynostosis subjects. Their findings have shown the displacement of the frontal bone away from the midsagittal plane, which can be considered as anterior fontanel expansion (as shown in this study). Examining the volumetric measures reported in Table 2 provides additional insight into the rapid changes occurring throughout the early postnatal development. The size of the anterior fontanel and total fontanel

area often increases during the first month of life before beginning to decrease, as shown in Table 2, possibly due to the rapid development of the brain hemispheres and the consequent outward growth of the calvarial bones. This fact was consistently reported in previous studies [7, 31]. Mercan et al. [7] have shown that the anteroposterior diameter slightly increases in the normal growth model. The results of intracranial volume measurement for the two age ranges are consistent with previous studies [32, 33] that showed the extent of intracranial volume in the post-natal normal group.

The potential limitation of the current study is that the restrictive age range of the sample limits the ability to examine skull developmental trajectories and rates of change. Extending the age range of the study to preterm neonates would provide more insight to brain and skull developmental profile. Moreover, it would provide the exact hard and soft tissue geometry required for clinical and research studies on preterm subjects. It would be also beneficial to extend this study on children up to 2 years old when bone ossification is completed. Finally, due to limited sample size, the other subject covariates, such as gender, cannot be considered in this study.

5 Conclusion

Subtle quantitative and qualitative assessment of neonate's skull shape and size during early infancy was reported in this study for identifying skull growth patterns in healthy neonates. Further studies using the age ranges below and above the age range covered in this study would be helpful in establishing a stereotactic skull development atlas.

6 Acknowledgement

This work was supported in part by the EGIDE France and the CISSC Iran under Grant 961/93-9-2 (Jundi Shapour Scientific Collaboration Program). The authors thank Mr. Omid Mehdizadeh

Dastjerdi for providing high quality neonate CT images. We would like also to thank Dr. Kamran Kazemi for sharing neonatal MR template and images.

References

1. Azizollahi, H., A. Aarabi, and F. Wallois, Effects of uncertainty in head tissue conductivity and complexity on EEG forward modeling in neonates. Hum Brain Mapp, 2016. 37(10): p. 3604-22.
2. Antonakakis, M., et al., The effect of stimulation type, head modeling, and combined EEG and MEG on the source reconstruction of the somatosensory P20/N20 component. Human brain mapping, 2019. 40(17): p. 5011-5028.
3. Kiesler, J. and R. Ricer, The abnormal fontanel. American family physician, 2003. 67(12): p. 2547-2552.
4. Gault, D.T., et al., Intracranial pressure and intracranial volume in children with craniosynostosis. Plastic and reconstructive surgery, 1992. 90(3): p. 377-381.
5. Ghadimi, S., et al., Skull segmentation and reconstruction from newborn CT images using coupled level sets. IEEE journal of biomedical and health informatics, 2015. 20(2): p. 563-573.
6. Sim, S.Y., S.H. Yoon, and S.Y. Kim, Quantitative analysis of developmental process of cranial suture in Korean infants. Journal of Korean Neurosurgical Society, 2012. 51(1): p. 31.
7. Mercan, E., R.A. Hopper, and A.M. Maga, Cranial growth in isolated sagittal craniosynostosis compared with normal growth in the first 6 months of age. Journal of anatomy, 2020. 236(1): p. 105-116.
8. Li, Z., et al., A statistical skull geometry model for children 0-3 years old. PloS one, 2015. 10(5): p. e0127322.
9. Aljabar, P., et al., Assessment of brain growth in early childhood using deformation-based morphometry. Neuroimage, 2008. 39(1): p. 348-358.
10. Momeni, M., et al., Neonatal Atlas Templates for the Study of Brain Development Using Magnetic Resonance Images. Current Medical Imaging Reviews, 2015. 11(1): p. 38-48.
11. Hashioka, A., et al., A neonatal brain MR image template of 1 week newborn. International journal of computer assisted radiology and surgery, 2012. 7(2): p. 273-280.
12. Dastjerdi, O., et al., Novel Multimodal Atlas Template for Spatial Normalization of Whole-Brain Images of Newborns. IRBM, 2016. 37(5-6): p. 254-263.
13. Ghadimi, S., et al., A neonatal bimodal MR-CT head template. PloS one, 2017. 12(1): p. e0166112.
14. Kuklisova-Murgasova, M., et al., A dynamic 4D probabilistic atlas of the developing brain. NeuroImage, 2011. 54(4): p. 2750-2763.
15. Momeni, M., et al., Temporal Resolvability Analysis of Macroscopic Morphological Development in Neonatal Cerebral Magnetic Resonance Images. Neuropediatrics, 2014. 45(04): p. 217-225.
16. Park, J.S., et al., A proposal of new reference system for the standard axial, sagittal, coronal planes of brain based on the serially-sectioned images. Journal of Korean medical science, 2010. 25(1): p. 135-141.

17. Kandel, E.I., Functional and stereotactic neurosurgery. 2012: Springer Science & Business Media.
18. Talairach, J. and P. Tournoux, Co-planar stereotaxic atlas of the human brain. 1988. New York: Theime, 1988.
19. Kazemi, K., et al., A neonatal atlas template for spatial normalization of whole-brain magnetic resonance images of newborns: preliminary results. Neuroimage, 2007. 37(2): p. 463-73.
20. Fedorov, A., et al., 3D Slicer as an image computing platform for the Quantitative Imaging Network. Magn Reson Imaging, 2012. 30(9): p. 1323-41.
21. Otsu, N., A Threshold Selection Method from Gray-Level Histograms. IEEE Transactions on Systems, Man, and Cybernetics, 1979. 9(1): p. 62-66.
22. Rorden, C., et al., Age-specific CT and MRI templates for spatial normalization. Neuroimage, 2012. 61(4): p. 957-65.
23. Avants, B.B., et al., A reproducible evaluation of ANTs similarity metric performance in brain image registration. NeuroImage, 2011. 54(3): p. 2033-2044.
24. Avants, B.B., et al., The Insight ToolKit image registration framework. Front Neuroinform, 2014. 8: p. 44.
25. Avants, B.B., et al., Symmetric diffeomorphic image registration with cross-correlation: evaluating automated labeling of elderly and neurodegenerative brain. Med Image Anal, 2008. 12(1): p. 26-41.
26. Avants, B.B., et al., The optimal template effect in hippocampus studies of diseased populations. Neuroimage, 2010. 49(3): p. 2457-66.
27. Avants, B. and J.C. Gee, Geodesic estimation for large deformation anatomical shape averaging and interpolation. Neuroimage, 2004. 23 Suppl 1: p. S139-50.
28. Ashburner, J. and K.J. Friston, Voxel-based morphometry--the methods. Neuroimage, 2000. 11(6 Pt 1): p. 805-21.
29. Popich, G.A. and D.W. Smith, Fontanels: range of normal size. The Journal of pediatrics, 1972. 80(5): p. 749-752.
30. Mathur, S., et al., Anterior fontanel size. Indian pediatrics, 1994. 31(2): p. 161-164.
31. Esmaeili, M., et al., Fontanel size from birth to 24 months of age in Iranian children. Iranian journal of child neurology, 2015. 9(4): p. 15.
32. Dekaban, A.S., Tables of cranial and orbital measurements, cranial volume, and derived indexes in males and females from 7 days to 20 years of age. Annals of Neurology: Official Journal of the American Neurological Association and the Child Neurology Society, 1977. 2(6): p. 485-491.
33. Abbott, A.H., et al., CT-determined intracranial volume for a normal population. J Craniofac Surg, 2000. 11(3): p. 211-23.

Figures

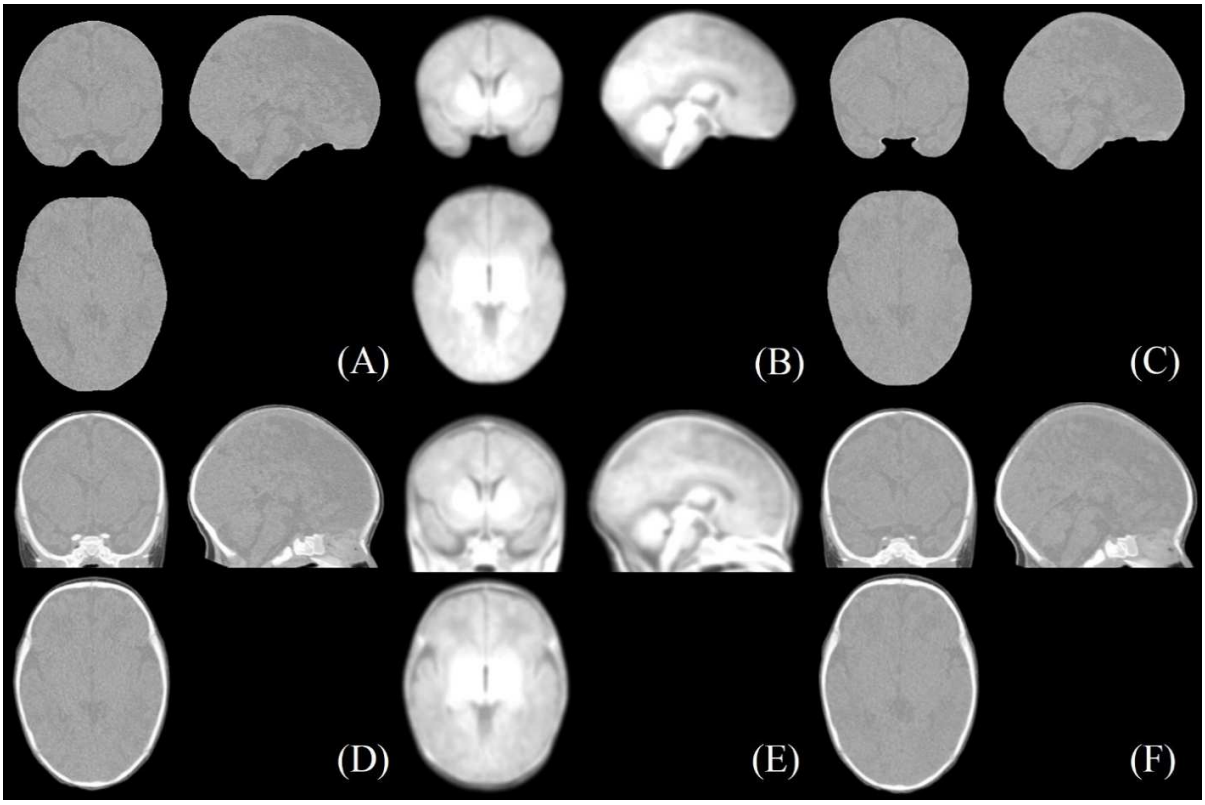

Figure 1. Mapping CT image to neonatal MR template. (A) CT image intracranial, (B) MR intracranial template [13], (C) Normalized CT intracranial to MR intracranial using affine and non-linear SyN transformation [25], (D) CT' image obtained by applying the resulting deformation field from normalizing (A) to (B) to the whole intensity transformed preprocessed CT image, (E) GRAMFC_$T_{39\text{-}42}$ MR template [19], (F) Fully registered CT image to MR template obtained by linearly registering (D) to (E).

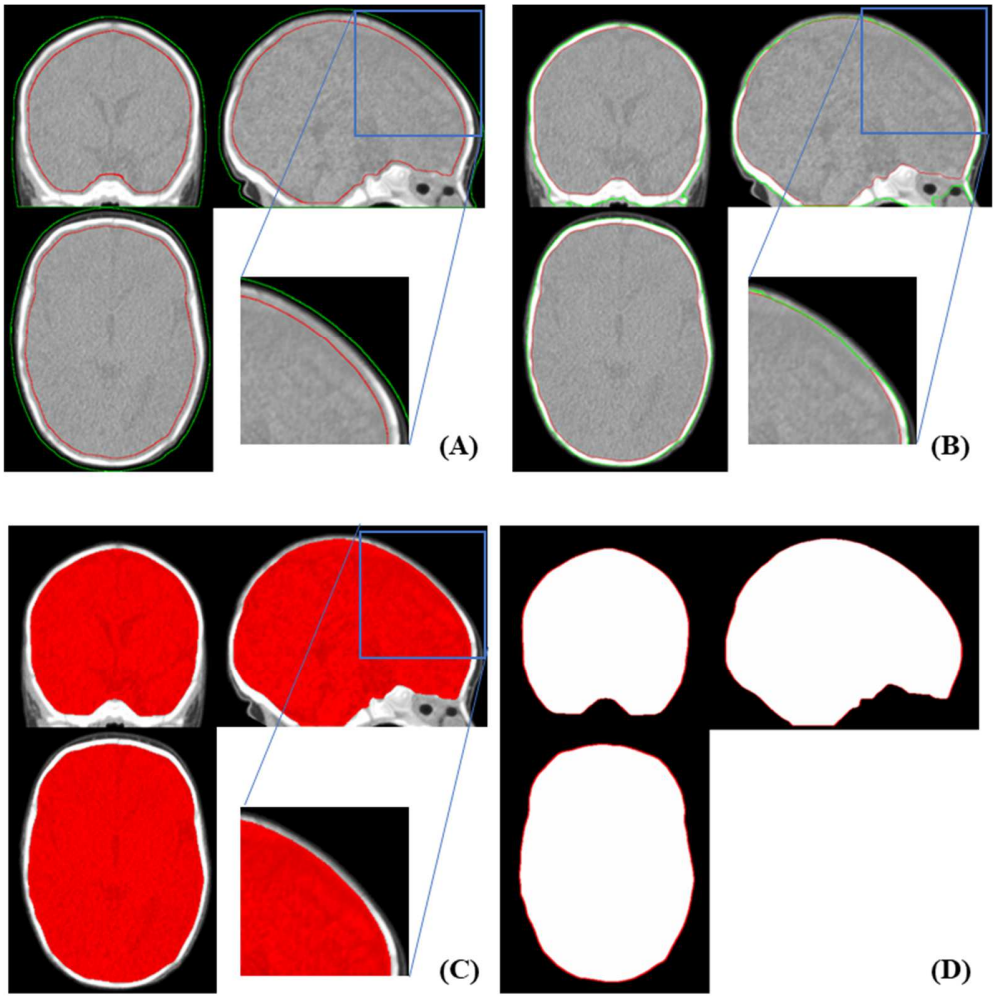

Figure 2. CT intracranial and skull surface extraction using the coupled level sets method described in [5]. (A) The initial interior (red) and exterior (green) surfaces. (B) The extracted inner and outer borders of cranial bones and reconstructed fontanels and sutures (C) Corresponding mask of the resulting interior contour using filling operator overlaid on the CT image. (D) The extracted intracranial mask; its volume is reported as intracranial volume.

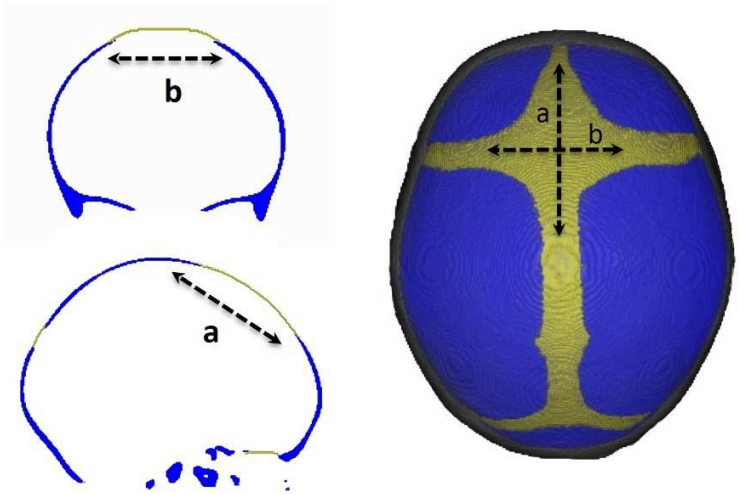

Figure 3. Anterior fontanel size is computed by averaging its anterior-posterior (a) and transverse (b) dimension.

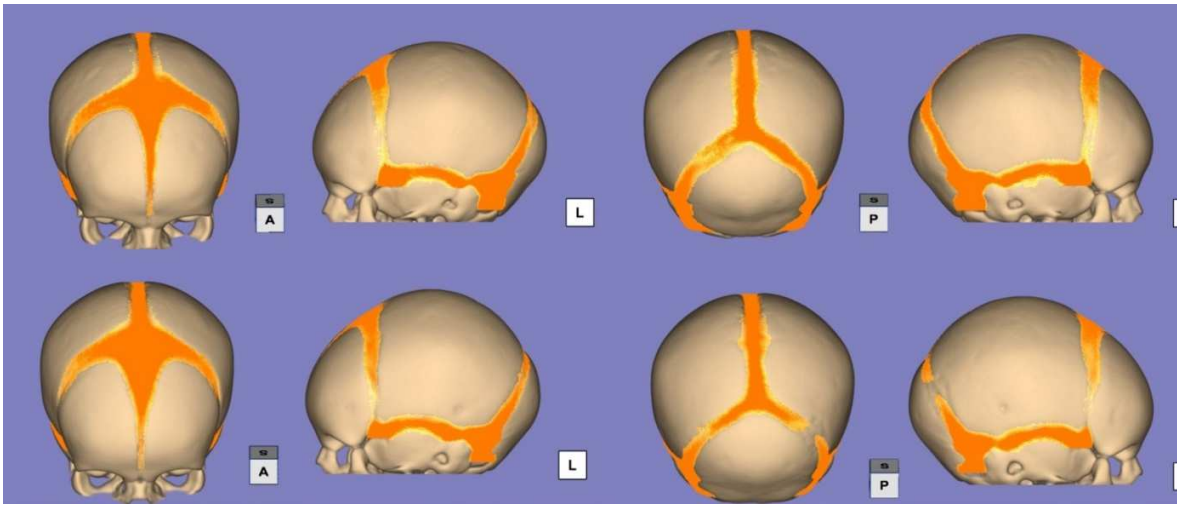

Figure 4. 3D surface visualization of cranial bone probability map and reconstructed fontanels and sutures for CT template with 39-40 weeks GA (first row) and CT template with 41-42 weeks GA (second row).

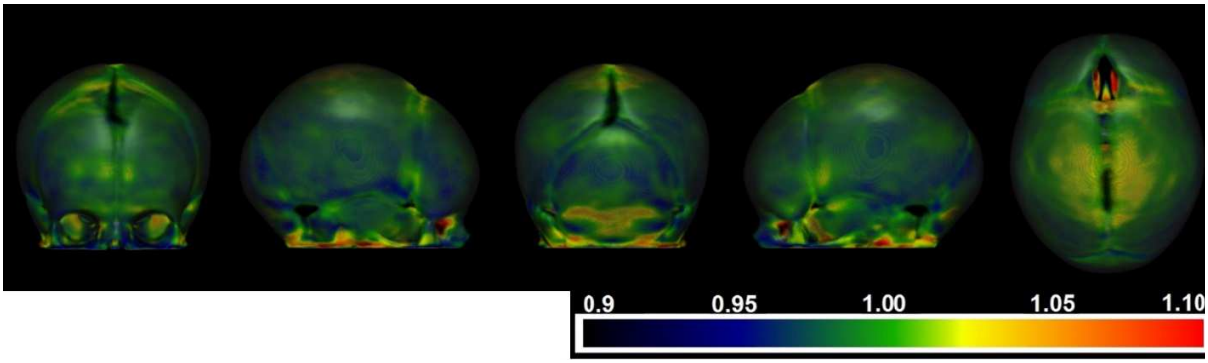

Figure 5. Local relative volume changes derived from nonlinear deformation that warps $CT_{39\text{-}40}$ towards $CT_{41\text{-}42}$. The gradient of the deformation field, also called the Jacobian matrix field, is then used to quantify local relative volume changes. The scale bar shows the determinant of the Jacobian matrix that is color coded to show regions of volume expansion ($|J|>1$), volume shrinkage ($|J|<1$) or no volume change ($|J|=1$).

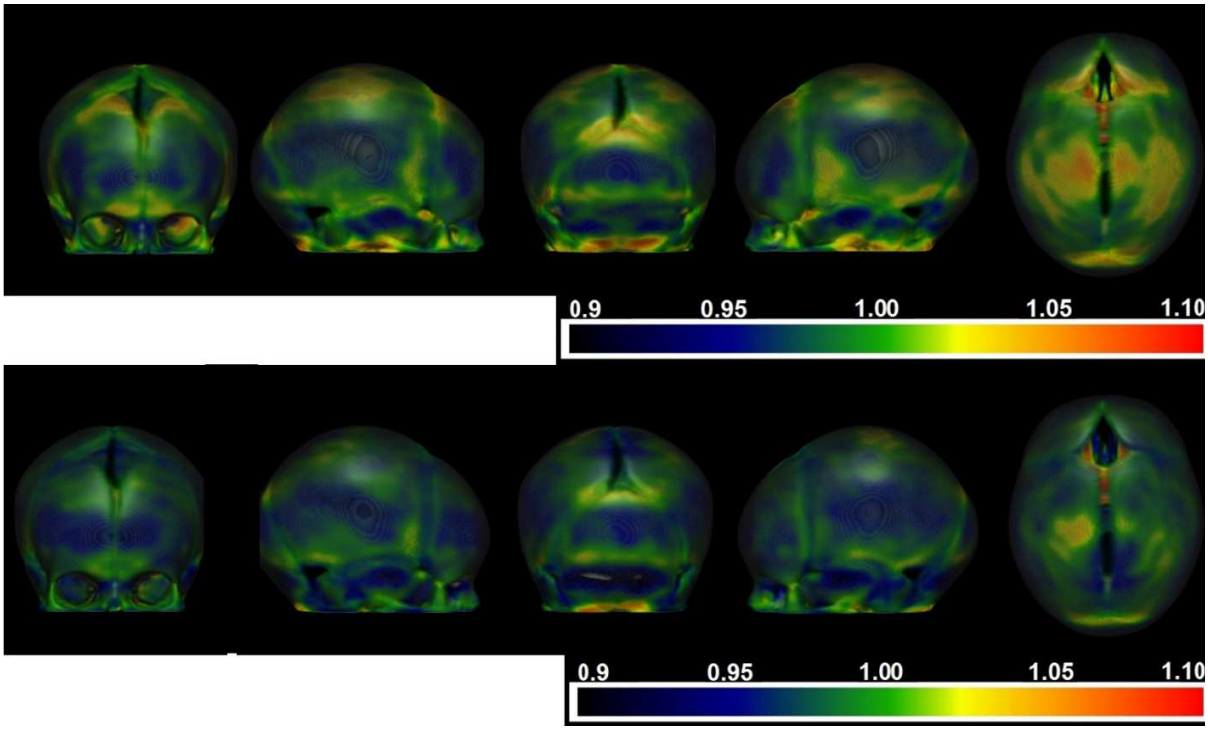

Figure 6. Local relative volume changes for subjects at 39-40 weeks GA (first row) and subjects at 41-42 weeks GA (second row) with respect to CT template at 39-42 weeks GA as a common coordinate system. Local relative volume changes in each row were calculated by averaging individual determinant of the Jacobian matrix. The Jacobian matrix field was derived from nonlinear deformation that warps each individual towards $CT_{39\text{-}42}$. The scale bar shows the determinant of the Jacobian matrix that is color coded to show regions of volume expansion ($|J|>1$) ,volume shrinkage ($|J|<1$) or no volume change ($|J|=1$).

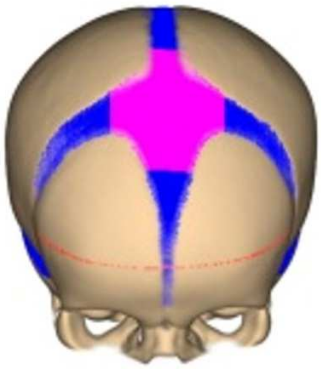

Figure 7. 3D surface visualization of the cranial bone probability map, anterior fontanel area (colored in pink), reconstructed fontanels and sutures by proposed algorithm in [5] (colored in blue) and scalp eliminated head circumference of the CT template (red line).

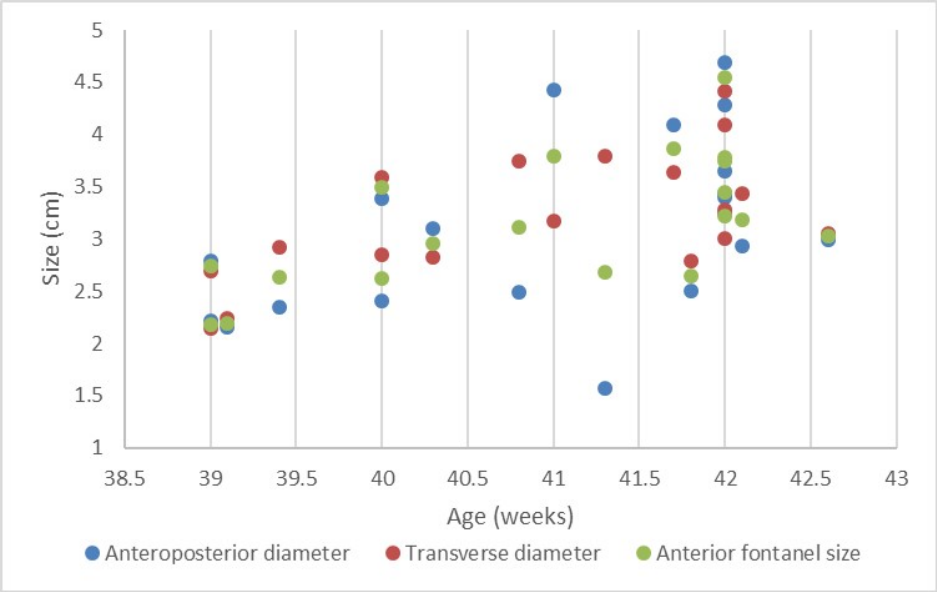

Figure 8. Anteroposterior diameter (blue dot), Transverse diameter (red dot) and Anterior fontanel size (green dot) measured in nineteen newborns aged from 39 to 42 weeks GA. Anteroposterior and transversal diameter are assumed to be the length of largest fontanel and sutures in sagittal and coronal view of individual CT images respectively. The anterior fontanel size is the average of anteroposterior and transversal diameter.

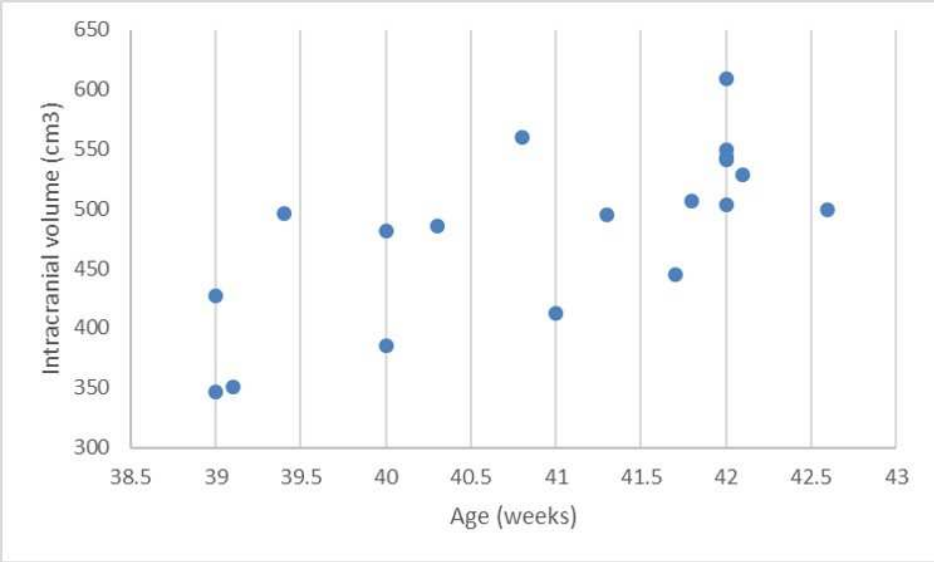

Figure 9. Intracranial volume measured in nineteen newborns aged from 39 to 42 weeks GA. For each individual, the mask of inner surface is derived by applying coupled level set approach for skull segmentation and fontanel reconstruction [5] and its volume is assumed to be the intracranial volume.